PCCP

ROYAL SOCIETY OF CHEMISTRY

PAPER

View Article Online
View Journal

Cite this: DOI: 10.1039/d1cp02917g

Isolating key reaction energetics and thermodynamic properties during hardwood model lignin pyrolysis†

Tanzina Azad,[a] Hazl F. Torres,[a] Maria L. Auad,[ab] Thomas Elder [c] and Andrew J. Adamczyk *[a]

Received 28th June 2021,
Accepted 13th September 2021

DOI: 10.1039/d1cp02917g

rsc.li/pccp

Computational studies on the pyrolysis of lignin using electronic structure methods have been largely limited to dimeric or trimeric models. In the current work we have modeled a lignin oligomer consisting of 10 syringyl units linked through 9 β-O-4′ bonds. A lignin model of this size is potentially more representative of the polymer in angiosperms; therefore, we used this representative model to examine the behavior of hardwood lignin during the initial steps of pyrolysis. Using this oligomer, the present work aims to determine if and how the reaction enthalpies of bond cleavage vary with positions within the chain. To accomplish this, we utilized a composite method using molecular mechanics based conformational sampling and quantum mechanically based density functional theory (DFT) calculations. Our key results show marked differences in bond dissociation enthalpies (BDE) with the position. In addition, we calculated standard thermodynamic properties, including enthalpy of formation, heat capacity, entropy, and Gibbs free energy for a wide range of temperatures from 25 K to 1000 K. The prediction of these thermodynamic properties and the reaction enthalpies will benefit further computational studies and cross-validation with pyrolysis experiments. Overall, the results demonstrate the utility of a better understanding of lignin pyrolysis for its effective valorization.

Introduction

Lignocellulosic biomass is one of the many resources for producing renewable energy but the only source for renewable biochemicals and biomaterials. Therefore, the development of renewable energy, chemicals and materials utilizing lignocellulosic biomass as an alternative to fossil fuel is important for a future secured both economically and environmentally. Lignin valorization has been an active area of research for many decades; however, a few factors, including the recent advancement in analytical tools, increased computational capacity, and the pressing issue of global warming, have motivated this research field to grow significantly in recent years.[1–5] Among the current techniques to valorize biomass by conversion into fuels and chemicals, enzymatic techniques[6–9] and catalytic conversion[10–14] are promising. Pyrolysis is a thermochemical conversion process, which is considered as one of the most promising techniques to derive material and energy from lignocellulosic biomass.[15–19] Pyrolysis thermochemically converts biomass in the absence of oxygen into all three physical states-char (solid), bio-oil (condensable liquid) and non-condensable (gas).[20] Among the several pyrolysis processes, including conventional/slow, fast, vacuum and flash, fast pyrolysis is particularly useful for producing bio-oil. To develop a cost-competitive fast pyrolysis process for biomass conversion, accurate prediction of thermodynamic properties and kinetic parameters, as well as a more comprehensive knowledge of input structures, are essential.

The major components of lignocellulosic biomass are cellulose (33–51%), hemicellulose (19–34%), and lignin (20–30%), where this composition varies with plant species types.[21] Table 1 compares the content of these components that can be found typically in hardwood and softwood.

While cellulose and hemicellulose are polysaccharides, lignin is a hydrophobic polymer composed mainly of phenylpropanoid units. These phenylpropanoid units arise from the

[a] Department of Chemical Engineering, Auburn University, Auburn, AL, USA. E-mail: aja0056@auburn.edu
[b] Center for Polymer and Advanced Composites, Auburn, AL, USA
[c] United States Department of Agriculture (USDA) Forest Service, Southern Research Station, Auburn, AL, USA

† Electronic supplementary information (ESI) available. See DOI: 10.1039/d1cp02917g

Table 1 Typical composition found in soft and hardwood[22]

	Hardwood (%)	Softwood (%)
Cellulose	42 ± 2	45 ± 2
Hemicellulose	27 ± 2	30 ± 5
Lignin	28 ± 3	20 ± 4
Extractives	3 ± 2	5 ± 3

combinatorial oxidative free radical polymerization of three main cinnamyl alcohols, *para*-hydroxy coumaryl alcohol, coniferyl alcohol, and sinapyl alcohol.[23] Monomers derived from these alcohols are denoted as H, G, and S, respectively. The proportion of these monomers varies with the type of wood. The gymnosperms (softwood) are mainly composed of G unit content with small levels of H units, while the angiosperms (hardwood) have both the G and S units in varying proportions. Natural angiosperm lignin with the highest S unit content (85%) has been reported in kenaf bast fiber lignin. Attempts to control lignin structure have been done through genetic modifications. One such example is a poplar lignin with extremely high proportion of S units (97.5%) by overexpression of the ferulate 5-hydroxylase (F5H) gene,[24] the key enzyme involved in synthesizing the monolignol sinapyl alcohol.[25]

In addition to the canonical cinnamyl alcohols, several phenolics, ferulate esters, and a type of flavonoid have recently been reported as lignin monomers.[26–30] The process of lignification starts with the enzymatic dehydrogenation that generates phenoxy radicals, after which the process becomes purely chemical, without requiring enzymes.[26] These phenoxy radicals allow considerable delocalization of unpaired electrons, and with the progression of the coupling process, multiple reactive sites emerge. Consequently, lignin becomes a highly irregular polymer having diverse linkage types. Fig. 1 represents some of these monomers and linkage types that can be found in lignin. Among all the interunit linkages, the β-O-4′ linkage in softwood lignin has a relative abundance of 50%.[31] For hardwood lignin, this linkage is more predominant, ranging from 69–77%.[32–34] Consequently, this higher percentage of ether bonds makes hardwood more reactive, making hardwood as a potentially better substrate for reductive catalytic fractionation.[35,36]

The presence of several monomers linked with diverse linkage types makes lignin highly heterogeneous, which represents a considerable challenge to its valorization. This notwithstanding, the development of value-added products from lignin is vital in operating biomass-based biorefineries that are cost-competitive with petroleum refineries.[37] Therefore, extensive studies have been carried out to elucidate lignin's transformation, during pyrolysis despite this bewildering complexity. The common experimental practice for studying lignin pyrolysis is to perform pyrolysis in the lab-scale reactor and subsequent characterization of these collected products.[38] Along with thermogravimetric (TG) analysis, which is one of the most widely used analytical techniques for studying biomass pyrolysis and degradation, several advanced experimental techniques have been employed recently, including micro-pyrolyzer combined with gas chromatography (GC), mass spectroscopy (MS), and flame ionization detection (FID) method (Py-GC-MS/FID);[39] TG coupled with mass spectrometry (TG-MS) and TG coupled with Fourier Transform Infrared Spectroscopy (TG-FTIR);[40] different types of *in situ* spectroscopy including *in situ* FTIR,[41] *in situ* X-ray diffraction,[42] spatiotemporally resolved diffuse reflectance *in situ* spectroscopy of particles (STR-DRiSP),[43] and *in situ* ^{1}H-NMR spectroscopy.[44] Several experimental studies have been performed using analytical techniques on model compounds with the ubiquitous β-O-4′ linkage.[45–52] However, these studies only indirectly reflect lignin atomic-level structure since lignin structure varies depending on the nature of its extraction from the lignin–cellulose complex of the plant cell. In addition to experimental studies on model compounds, results from theoretical studies employing quantum chemistry[53] and molecular dynamics simulation[54–56] have been reported to reveal detailed steps in reaction mechanisms and provide insights on product distribution, predominantly for smaller model lignin species.

Lignin pyrolysis has been extensively studied using quantum chemical calculation with model dimers representing alkyl–aryl ether and condensed type linkages.[26,57–61] Studies including both analytical and theoretical results provide insights for the possible mechanisms involved in pyrolysis, *i.e.*, homolysis or heterolysis, since both reaction classes have been reported to occur in lignin pyrolysis. Klein and Virk proposed a retro-ene

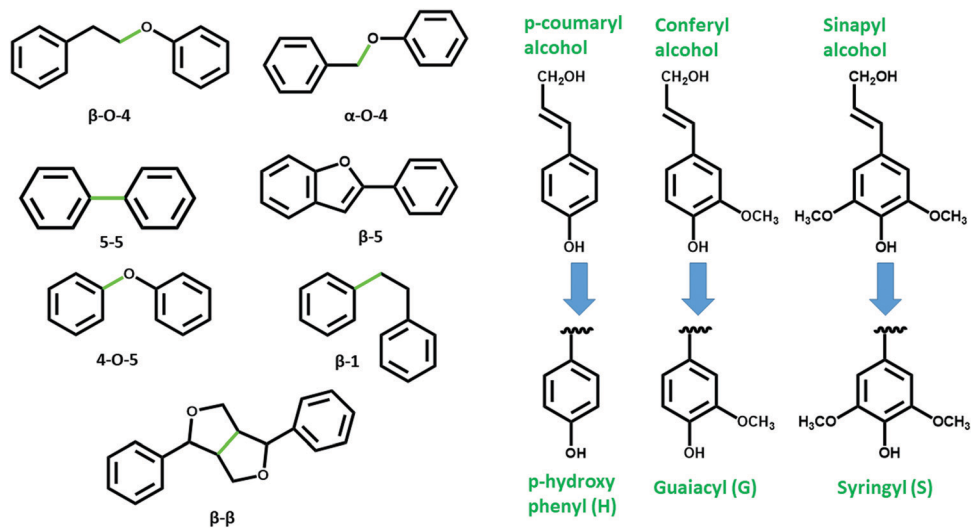

Fig. 1 Common linkages (left) and major monolignols (right) found in lignin.

mechanism based on the reaction kinetics to form styrene and phenol using the simplest model compound phenethyl phenyl ether.[62] In a separate study, the formation of degradation products from the gas-phase pyrolysis of the same model compound was investigated to conclude that the homolysis of C–O occurs at high temperatures (greater than 1000 °C). In contrast, the concerted retro-ene and Maccoll mechanisms occur at lower temperatures (less than 600 °C).[63] Low-temperature homolysis of the β-O-4′ bond *via* a quinone methide intermediate has been postulated under solvated[64,65] and steam-explosion conditions.[66] Lately, Density Functional Theory (DFT) studies combined with Py-GC/MS, HPLC/QTOF-MS, GPC and 2D HSQC NMR techniques have been reported for the pyrolysis of several model lignin compounds.[67,68] Selective cleavage of common linkages found in native lignin including the aliphatic C–O linkages[69] and C–C bonds,[70] and α-O-4 bonds[71] have been reported in the contemporary literatures using both experimental and computational tools. While there have been reports on the diverse linkage types thereby enriching the overall understanding of lignin chemistry, all of these electronic structure studies have been limited in size to dimeric to trimeric structures. The current work seeks to determine how or if the pyrolysis behavior of lignin, as evidenced by bond dissociation energies (BDEs), changes for a significantly larger model compound.

This study has applied contemporary computational methods to evaluate the reaction enthalpies associated with a syringyl 10-mer oligolignol connected through β-O-4′ linkages. The homolytic cleavage reaction event occurs as one of the initial reactions in lignin pyrolysis. In our previous work using electronic structure methods, we studied an oligomeric model structure for lignin, made of ten guaiacyl units, connected through β-O-4′ linkages, and identified marked position dependence in the calculated reaction enthalpies.[72] While the previous study revealed the position dependence of BDEs of a model representative of softwood lignin, this study aimed to investigate if such position dependence can be found in an oligomer mimicking hardwood lignin. Given such a large oligomer flexibility, classical molecular mechanics based conformational sampling, which was developed in our previous study, has been applied to generate lower energy conformational isomers. Subsequently, these lowest energy conformers have been used to determine BDEs employing density functional theory (DFT) and statistical thermodynamics calculations. Lastly, thermochemical properties, including enthalpy, entropy, free energy, and constant pressure heat capacity values, were estimated using conventional statistical thermodynamics formulas. Although we have studied a simplified model structure to test the aforementioned hypothesis, our predicted values for BDEs agree reasonably with other reported values in the literature of various origins, both experimental and computational. The predicted thermochemistry in this study provides insights for hardwood lignin thermodynamic properties using molecular modeling, which would be very useful for cross-validation with experimental studies.

Computational methodology

Reaction pathway schemes

Using the LigninBuilder Algorithm,[73] a decamer made up of ten syringyl monolignols were linked with the β-O-4′ bond type which is shown in Fig. 2(a). While this is an idealized structure, using such model lignin compound to investigate a specific question or hypothesis in lignin pyrolysis has been well documented in the literature.[74,75] Through overexpression of the ferulate 5-hydroxylase gene in poplar, Stewart *et al.* (2009)[24] produced lignins with very high syringyl content and molecular weights consistent with the oligomer under consideration in the current work. Furthermore, due to the presence of a methoxyl group at the C-5 position, the possible interunit linkages are limited to β–β resinols, and the β-O-4′ bond types, the latter of which was found by experiment to be dominant. As such, the β-O-4′ linked syringyl decamer in this paper represents a reasonable oligomeric model for lignin. While differing syringyl:guaiacyl ratios and bond type would be more realistic, in order to address the question of whether or not BDE varies with positions in the oligomer, the inclusion of such variability would have confounded the results, making it difficult or impossible to distinguish between the effect of position and bond type. Using such simplified structures is particularly common for lignin[36–39] where the experimental evidence for the structure, reactivity and degradation of the native polymer are limited and incomplete. In this work, a systematic homolytic cleavage of each β-O-4′ bond has been studied with the main objective to investigate whether or not BDE changes between these nine pathways originating from homolytic cleavage of the β-O-4′ bonds at nine different positions.

Conformational analysis

In this work, a conformational sampling method developed in our previous study[72] was used as an essential step to refine the input structures before DFT electronic structure calculations. The COMPASS force-field was used in this semi-automated sampling method where a stochastic conformational search was performed by applying the Boltzmann jump method, which uses the Metropolis Monte Carlo criterion[76] to accept or reject a jump in structural change due to torsional displacement. The COMPASS force-field was used for all structures, including the reactant closed-shell molecule and the free radical products. All bonds capable of torsion in the structures were rotated stochastically in a 10° range of torsional windows. Each conformational search step consisted of 1000 conformers from which the lowest energy conformer was selected as the input for the next search. The process was repeated until no statistically significant change in end-to-end distance was found between two consecutive conformer searches. Atom-based electrostatics and van der Waals (vdW) summation methods were used and performed with cubic spline truncation, employing a cutoff distance of 12.5 Å, a spline width of 1 Å, and a buffer width of 0.5 Å. Our results indicate that the COMPASS force-field is acceptable for determining the geometry inputs for the subsequent lignin polymer electronic structure calculations. It should be noted that

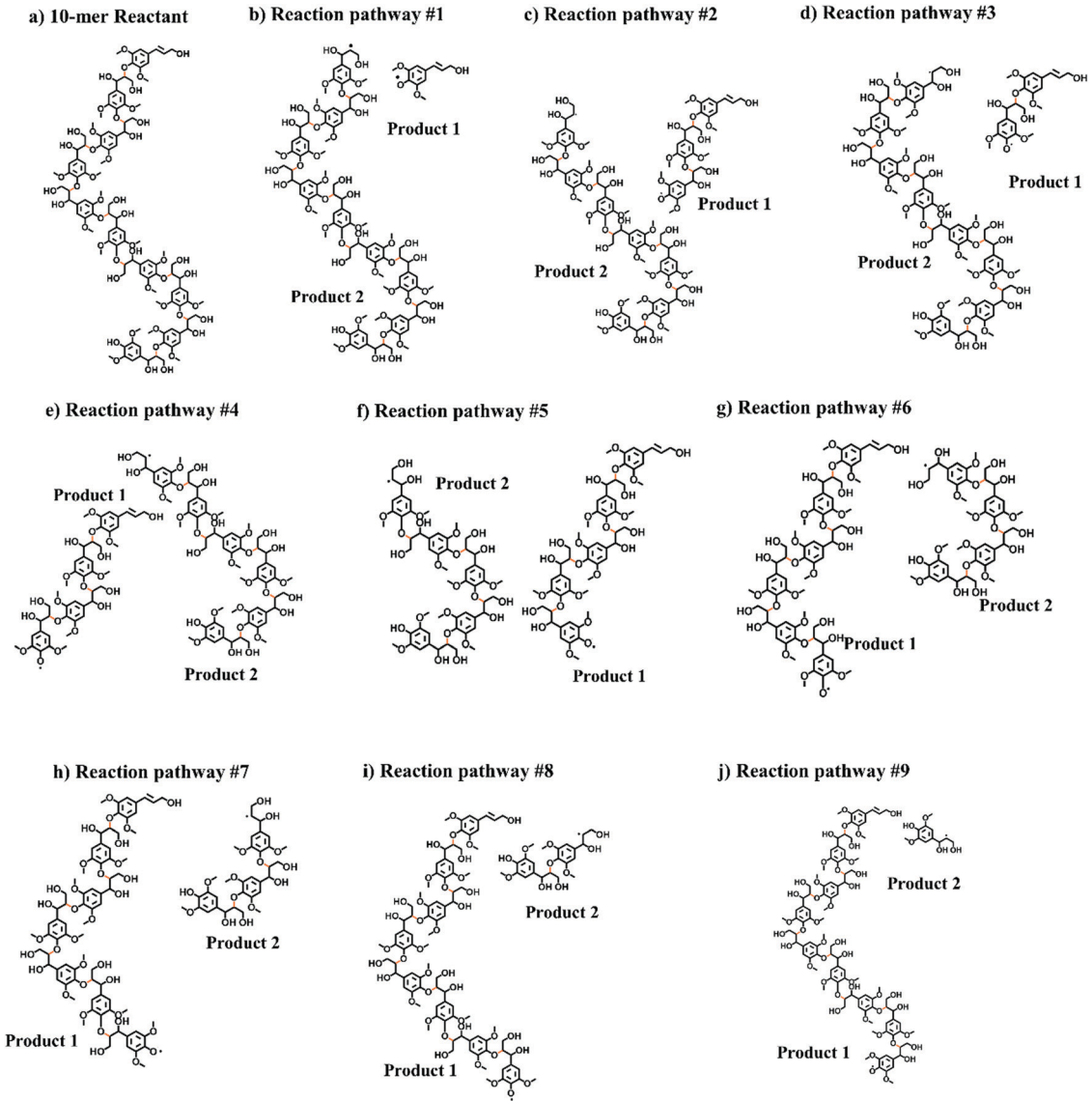

Fig. 2 (a) Initial reactant structure; (b–j) pairs of radical products generated along each of the nine reaction pathways for studying BDE of β-O-4′ in model lignin oligomer. Products 1 and 2 are radical fragments with the radical center on oxygen and carbon atoms, respectively.

reaching a global minimum is not guaranteed with this sampling method. However, local energy minima were obtained, which were used as improved inputs for DFT electronic structure calculations.

Electronic structure calculations

All electronic energies were calculated using DFT in the Dmol3 package considering all electrons for each atom with 4.4 Å global orbital cut-off energy.[53] A Generalized Gradient Approximation (GGA) type exchange correlation functional Becke–Lee–Young–Parr (BLYP)[77] was used. Based on the superior cost effectiveness of numerical basis sets in Dmol3 relative to Gaussian basis sets,[78] we used a numerical basis set of double zeta quality plus polarization functions (DNP). While the use of hybrid meta GGA functionals *e.g.* B3LYP and Gaussian basis sets have been well documented in similar BDE studies for smaller models of lignin, the accuracy of BLYP-DNP level of theory has been reported for studying reaction energetics and thermochemistry for organic compounds and biopolymers.[79–83] The Tkatchenko–Scheffler (TS) method was used for DFT-D correction to include nonbonded interactions.[84] Taking the lowest energy conformation for all structures, geometry optimization was done at BLYP-DNP level where the convergence criteria were 2×10^{-5} Hartrees (Ha) for total energy, 0.004 Ha $Å^{-1}$ for the maximum force of every atom, and 0.005 Å for maximum displacement. The self-consistent-field (SCF) tolerance was set to be 1×10^{-5} Ha. Small inorganic systems with similar reactive features to this work have been extensively studied with success in our group using comparable hybrid methodologies.[85–89]

After geometry optimization at BLYP-DNP level, vibrational frequency calculations for all structures were performed at the same level of theory to determine the thermochemical properties, enthalpy (H), entropy (S), free energy (G), and heat capacity

at constant pressure (Cp). The values for these properties as functions of temperature were obtained from standard statistical thermodynamics using molecular partition functions based on the harmonic oscillator and rigid rotor approximations for polyatomic gas molecules.[90] Details on the calculation of these properties including the electronic, translational, rotational and vibrational contributions for the molecular partition functions can be found in the ESI.† Also, the Dmol3 package was used to calculate additional properties including electron density and molecular orbitals which were used to describe the stabilization of product free radicals.

Bond dissociation enthalpies

Unlike most BDE studies, we employed the values of standard enthalpies of formation from the calculations of statistical thermodynamics to calculate BDEs. In our study, we calculated BDEs at the reference temperature as the difference of the sum of the standard enthalpies of formation of the product fragments and the standard enthalpy of formation of the reactant, as shown in eqn (1),

$$\mathrm{BDE}_{298\ (\mathrm{Reaction\ pathway})} = \left[\Delta H^{\circ}_{\mathrm{f},298(\mathrm{Product\ 1})} + \Delta H^{\circ}_{\mathrm{f},298(\mathrm{Product\ 2})}\right] - \Delta H^{\circ}_{\mathrm{f},298(\mathrm{Reactant})} \quad (1)$$

where $H^{\circ}_{\mathrm{f},298}$ is the standard enthalpy of formation of the radical species Products 1 and 2, and the reactant is the original lignin 10-mer. A hybrid methodology based on quantum chemical calculations, statistical thermodynamics and experimental values for atomization energies was used to calculate the values for enthalpies of formation, as performed in previous work from our group.[85] The enthalpy of reaction at elevated temperature, *i.e.*, BDE at temperature T, is then calculated using the calculated $\mathrm{BDE}_{298\mathrm{K}}$ and temperature-dependent heat capacity values using eqn (2),

$$\mathrm{BDE}_T = \mathrm{BDE}_{298\,\mathrm{K}} + \int_{298\,\mathrm{K}}^{T} \Delta C_{\mathrm{P,Rxn}}(T)\mathrm{d}T \quad (2)$$

$\Delta C_{\mathrm{p,Rxn}}(T)$ is the temperature-dependent polynomial defined as the difference between the sum of the temperature-dependent standard heat capacities of the products and the temperature-dependent standard heat capacity of the reactant. The details of heat of formation as well as the other standard thermodynamic properties calculation structure for each can be found in the ESI.†

Results and discussions

Conformational analysis

Each geometry used as an input for quantum mechanical calculations should be the lowest energy conformer to ensure best accuracy in the results obtained from quantum mechanical calculations. Therefore, conformational search was a preliminary refinement step to study our large and flexible hardwood model lignin oligomer generated for this work. Conformational information is of significance for all the processes including biomass pyrolysis for several reasons. Firstly, conformational information provides a more accurate understanding of the structure, which is crucial for lignin, which unlike cellulose lacks a well-defined structure. The role of substituents in the model structures for lignin can be significantly better understood if a large conformational space of model structures is considered.

The conformational analysis of the model lignin structures using our developed sampling method indicates that the starting conformation for all the structures, *i.e.*, closed or open shell, has no role in generating the lowest energy conformers for these two types of structures. Instead, folded refined structures with minimized energy, which are the conformational sampling step outputs, largely depended on the molecular weight and the polymer chain length. Furthermore, the obtained lowest energy conformers showed no selectivity trend for the β-O-4′ bond cleavage position and the cleaved product fragment stereochemistry. For both radical-containing fragments (product 1 and 2), not the radical center position, but the amount of non-bonded interactions played a significant role in generating the lowest energy conformers. Fig. 3 shows all of the lowest energy conformers for the reactant molecule and the two types of product structures generated using our conformational sampling method. Subsequently, each of these structures were geometry optimized at BLYP/DNP level for DFT electronic structure calculations.

Conformational landscape

We built an extensive library of lignin conformational isomers and found the lowest energy conformers using our previously developed sampling method. This lignin library has a database of model structures ranging from 1-mers to 9-mers of open-shell species and a decamer of closed-shell structures. In the current study, the number of rotatable dihedral angles in the smallest radical species was five, both for product 1 and 2 structures, while it was 61 for the most flexible radicals belonging to product 1 and 2 types. The number of dihedral angles stochastically selected and rotated for the decamer reactant closed-shell molecule was 68. Due to the high numbers of rotatable bonds in this flexible model lignin structure, we did not use systemic grid search to avoid the combinatorial explosion for possible numbers of conformers to be generated, even though it could provide us the global energy minima for all structures. Therefore, this work used a stochastic conformer search using the Metropolis MC-based sampling method to find reasonable local minima to be used as the inputs for higher-level quantum chemical calculations. Ideally, it would be more accurate if we could investigate the multiple lowest energy structures obtained from this random sampling with subsequent DFT calculation for BDE analysis. However, this requires extensive calculations of these conformers, which is beyond the scope of this study. We anticipate that this extensive BDE calculation with DFT employing multiple lowest energy conformers for each structure could provide exciting statistical analysis results. Since the overall objective of using this sampling method was to improve the

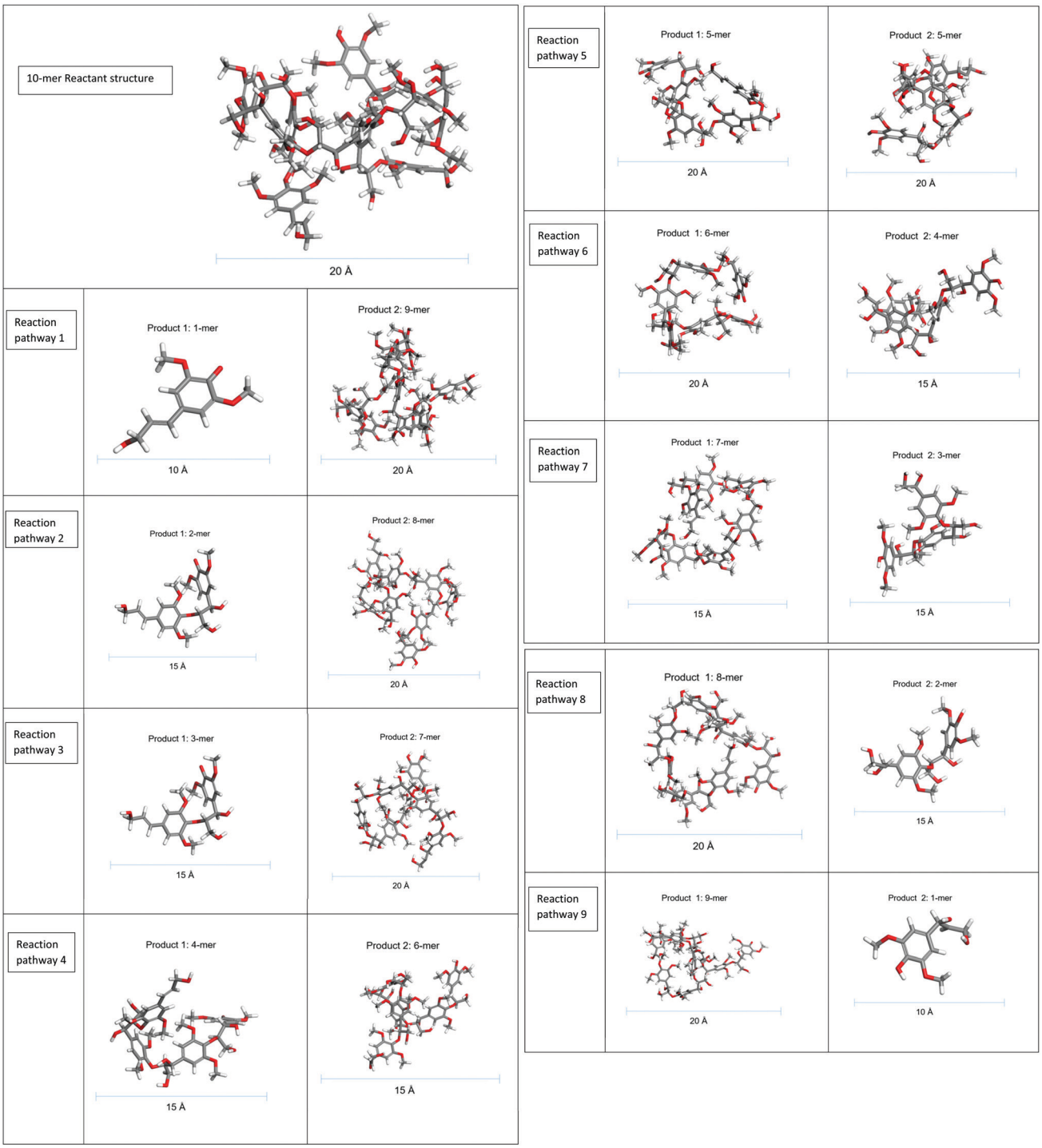

Fig. 3 Optimized structures for all products and the reactant at the BLYP/DNP level of theory for this study.

geometries for quantum chemical calculations, the local minima generated using this method were used to test the specific significant hypothesis aforementioned in the Introduction section.

Bond dissociation enthalpies

The elementary reaction under investigation involves a free radical formation that has been identical for all pathways. Due to the homolysis of the C–O bonds in the β-O-4′ linkage at the different positions, transient species of different molecular weights were formed as the products, all of which have radical centers at the edge of the polymer chain. The initial conformation for all structures was not seen to be conserved, which can be explained by considering the need to stabilize the exposed radical centers for product structures and energy reduction for the reactant structure as an outcome of conformational sampling.

Table 2 Bond dissociation enthalpy values for each reaction pathway studied in the current work for a model S-lignin decamer

Reaction pathway	Calculated BDEs values for 25–1000 K (kcal mol^{-1})	BDE value at 298 K (kcal mol^{-1})
1	69.09–80.11	72.14
2	58.92–74.99	62.68
3	45.89–60.90	49.29
4	47.81–56.28	49.42
5	67.48–63.77	67.86
6	66.46–68.81	67.11
7	77.66–70.05	76.45
8	64.30–59.01	64.23
9	68.08–65.34	68.13

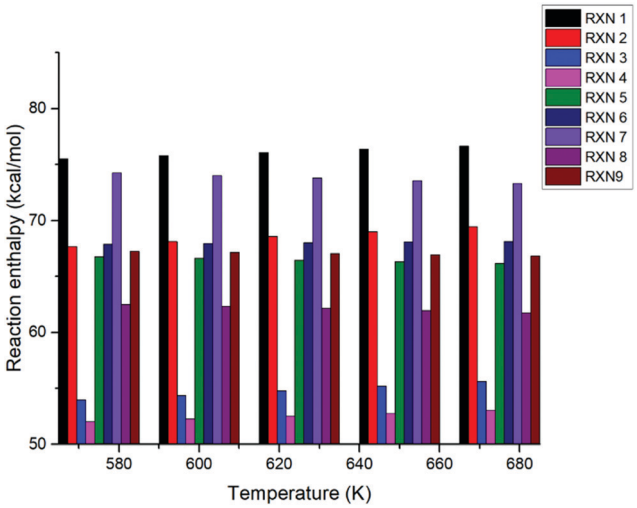

Fig. 4 BDE values for the homolytic β-O-4′ cleavage reaction in hardwood model lignin decamer at different positions under selected temperature range of primary pyrolysis.

Since non-bonded interaction includes interactions for all possible pairs of non-bonded atoms, an additional methoxy group in each benzene ring for the syringyl monolignol increased the role of the overall non-bonded interactions for the hardwood model lignin oligomer compared to the softwood model oligomer having only guaiacyl monolignols. The lowest energy conformers used as the inputs for DFT electronic structure calculations to evaluate the BDEs along different pathways had different non-bonded interaction energies, which arose from the difference in radical stabilization. Therefore, a significant position dependence has been observed along the pathways studied for the BDE calculations in this work. Table 2 lists the range of BDEs and the BDE calculated at the reference temperature of 298 K for this work.

As mentioned previously, 9 distinct reaction pathways were obtained after homolysis of β-O-4′ bonds at 9 different positions along the model lignin decamer. For reaction pathway 1, BDE varied from 69.09 to 80.11 kcal mol^{-1} over the temperature range 25–1000 K. In terms of the product sizes, reaction pathway 9 was similar to this pathway, but the range of BDE calculated for this pathway was found as 65.34–68.08 kcal mol^{-1}. This trend indicates that over the temperature range of 25–1000 K, reaction pathway 1 yields a relatively wider BDE range than pathway 9. Similar to the temperature dependence observed in pathway 1, *i.e.*, 11.02 kcal mol^{-1} reaction enthalpy variation over 25–1000 K range, pathways 2, 3, 4, and 7 showed marked temperature dependence for the reaction enthalpies. Among these, pathway 2 has the largest temperature dependence of 16.07 kcal mol^{-1} over the entire temperature range. While pathways 1–4 showed a temperature dependence with an increasing trend in reaction enthalpy with an increase in temperature, pathway 7 exhibited a decreasing trend in endothermicity with the temperature rise. A variation of 7.6 kcal mol^{-1} in reaction enthalpy was obtained along this pathway from 25 K to 1000 K. Similar to pathway 7, reaction pathway 8 showed a 5.3 kcal mol^{-1} variation in reaction enthalpy with a decreasing BDE trend with the increase in temperature. Along 3 pathways, namely, 5, 6, and 9, the variations of reaction enthalpy as a function of temperature were very small, indicating negligible temperature dependence of reaction enthalpies. Among these 3 pathways, pathway 6 showed the lowest temperature dependence with only 2.35 kcal mol^{-1} variation in the reaction enthalpy. Fig. 4 shows the position dependence of BDEs calculated in this study for temperature range of 300–400 °C, which is the range of primary pyrolysis temperature of lignin.

One of the objectives for the current work was to investigate the effect of increased non-bonded interaction energy for the hardwood model lignin decamer, which was generated using a syringyl monolignol. The structural difference between our hard- and softwood model lignin decamer lies in the presence of an additional methoxy group in each repeating unit of the hardwood model. Consequently, between these two model oligomers, the role of non-bonded interactions in conformational sampling and the BDE calculations have been much more prevailing in the hardwood system than the softwood (shown in Fig. S7, ESI†). This trend can be observed from our comparison between BDE calculations for these two systems.

The position and temperature dependence of BDE for the homolytic cleavage of the β-O-4′ bond found in this study were also observed similarly in our previous study where we used the same level of theory, *i.e.*, BLYP/DNP for geometry optimization and vibrational frequency calculations.[72] At the reference temperature of 298 K, calculated BDEs were 64.4, 50.1, 65.4, 54.4, 62.1, 63.0, 69.6, 57.5 and 59.3 kcal mol^{-1}, along 9 reaction pathways in our previous study for a model lignin oligomer mimicking softwood lignin. Fig. S6 (in the ESI†) compares our prediction for softwood and hardwood model lignin BDE for homolytic cleavage of the β-O-4′ bond at the reference temperature. Comparing these two complementary works, our results indicate a slightly wider position dependence of hardwood model lignin decamer BDE for homolytic cleavage of the β-O-4′ bond, which was studied in the current work. For example, at the 298 K temperature, pathway 3 showed a BDE of 49.29 kcal mol^{-1}, the lowest calculated BDEs among the 9 pathways for our current study with hardwood model lignin. The highest BDE of 76.45 kcal mol^{-1} was found along pathway 7 in the current study. In our previous study with softwood model lignin, the lowest BDE was found as 50.1 kcal mol^{-1} for

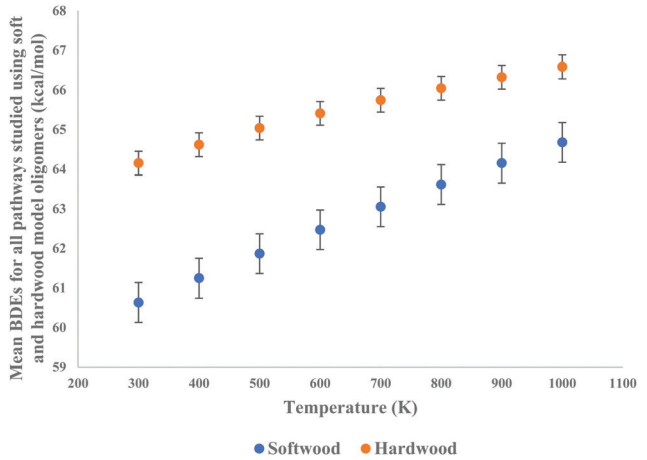

Fig. 5 Comparison between mean BDEs calculated in two model oligomers mimicking softwood and hardwood at selected temperature. The error bars show the standard error of the mean for the calculated BDEs.

pathway 2, and the highest BDE was found as 69.6 kcal mol^{-1} for pathway 7, at the same reference temperature. At all temperatures, mean BDEs calculated for each the 9 reaction pathways studied with hardwood model lignin decamer was higher than that of the softwood model lignin decamer, shown in Fig. 5. This trend is an interesting finding that aligns with our expectation that, comparatively, BDE is higher in hardwood model lignin than softwood model lignin. Here, the only difference in these two model decamers lies in the monolignols used, that is, the hardwood model lignin has an additional electron donating group in each monomer.

Although variation in the mean BDEs have been observed using the softwood and hardwood model lignin decamers, these variations are not statistically significant at the 95% confidence interval. A paired two tailed *T*-test was used to check if the observed variations between the mean BDEs are statistically significant, detailed calculation of which has been included in the Table S11 (ESI†). However, the variation in BDE along the oligomer chain, that is, as a function of position or reaction pathway for both hardwood and softwood model lignin was found to be statistically significant.

Comment on level of theory selection

Very high-level *ab initio* methods, including CCSD(T) and QCISD(T)/6311G(d,p) methods, as well as various composite methods such as G2, have been reported to accurately reproduce BDEs that are within 4–8 kJ mol^{-1} from the experimentally obtained BDEs.[91–96] However, the inherent limitation of these high-level methods prevents their application beyond small molecules. As a result, DFT techniques have been well studied for predicting BDEs, especially for lignin, given its polymeric nature. Lower level methods, such as a semiempirical calculation followed by the DFT method, for example, AM1 and B3LYP/6-31G(d), have been suggested for geometry optimizations.[97–99] According to these studies, B3LYP, which is the highest used functional for studying BDE of smaller lignin models, underestimates the BDE value. Another hybrid method, namely, KMLYP, has been suggested to calculate BDE with DFT methods,[100,101] even though the accuracy of KMLYP for predicting lignin BDE has not yet been reported.

Table 3 Comparison of the mean BDE computed at the reference temperature in this study with the contemporary theoretical studies

Ref.	Reported BDEs at 298 K (kcal mol^{-1})	Deviation from the mean BDE calculated at 298 K in this study	% Deviation
58	69.2	5.06	7.31
57	67.3	3.16	4.70
59	57.1	−7.04	−12.33
61	68.8	4.86	7.06
103	54.5	−9.64	−17.69
102	61.5	−2.74	−4.46
104	65.8	1.66	2.52

The present study has used a lower level functional BLYP due to the relatively large model oligomer structure. Other higher level functionals might predict more accurate BDE results, where accuracy level is defined in the context of the Jacob's ladder for systematic improvement of DFT introduced by Perdew. However, the BLYP functional was used in this work due to affordable computational power, a critical criterion given the large system size investigated. The accuracy of BLYP/DNP level has been reported for studying the reaction energetics and thermochemistry for organic and bio-polymer model compounds.[80–83] Contemporary BDE studies of lignin use different model compounds and different levels of theory for DFT calculations, limiting the comparison of our results directly with these reported BDE values. However, it is to be highlighted that our BDE values calculated at the BLYP-DNP level are within the range of BDE values predicted in other studies (shown in Table 3). Despite using this lower level functional, our predicted BDEs match with other reported values, all of which used DFT methods with higher level functionals.[57–61,102–104] For instance, BDE results for the β-O-4′ bond cleavage reaction of the closest model structure resembling our study dimer were reported as 69.2 kcal mol^{-1} using the M06-2X/6-31G(d) level of theory.[58] To the best of our knowledge, the BDEs in the current hardwood model study represents the largest lignin oligomer for which electronic structure methods have been used to determine the bond dissociation enthalpies following a branching mechanism, which has been shown in Fig. 6.

Factors contributing to the stability of radicals

The homolytic cleavage reaction of the β-O-4′ linkages in our system yielded phenoxy radicals and carbon-free radicals (Fig. 2b–j). The C atom has tetrahedral hybridization for all the C–O bonds that we have cleaved in our study. Both the hybridization type and the nature of substitution have effects on the BDEs. Both types of radical products have the same substitution as well. The radical center is on the O atom attached to the benzene ring for the phenoxy radicals, which has two methoxy groups in the two adjacent ortho positions. These phenoxy radicals have a secondary C atom in the para position. The side chain attached to this C atom increased with

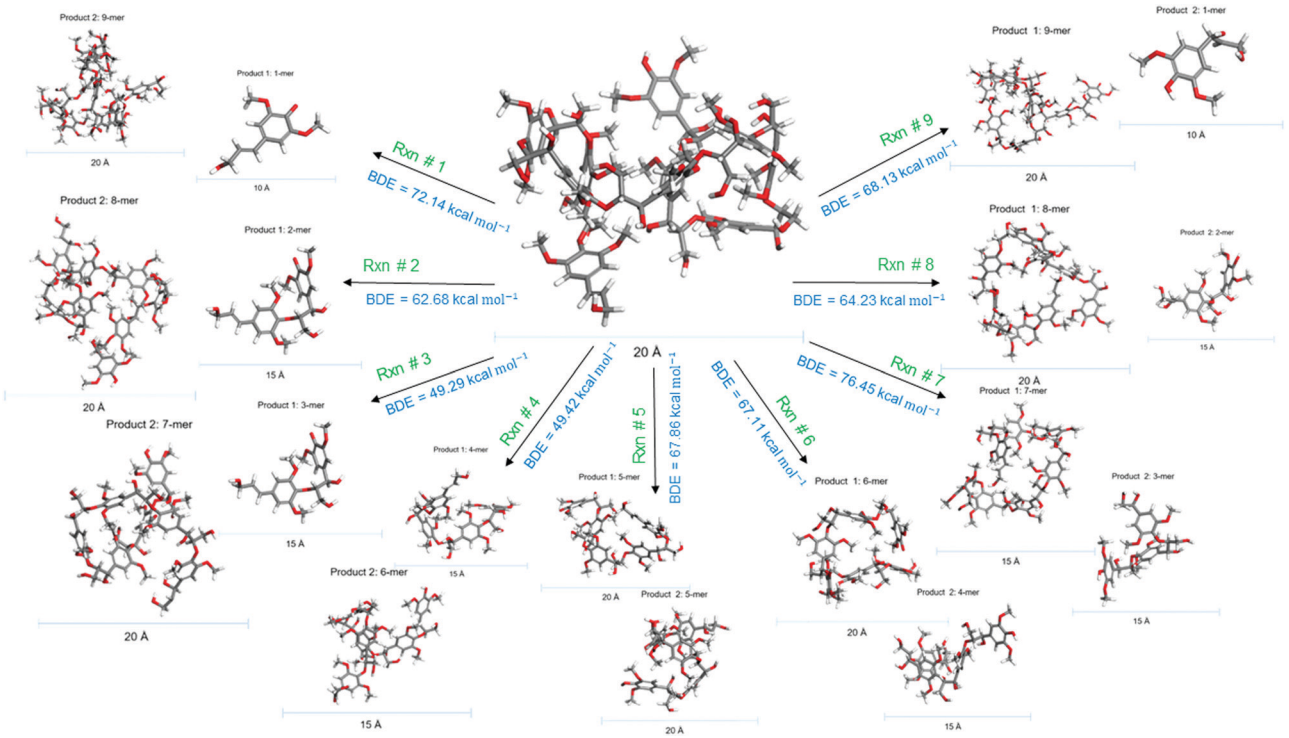

Fig. 6 Bond dissociation enthalpies calculated following a branching reaction mechanism using the hardwood model lignin oligomer. The different reaction enthalpy values along different reaction pathways depict the position dependence of the homolytic cleavage of β-O-4 bonds in the model oligomer.

the increase in structure size for product 1. Similar to phenoxy radicals, the type of hybridization and substitution remained the same for the carbon-free radical type species (product 2 species). In all product 2 structures, the radical center is attached with a methylene functional group at one end and with an additional secondary C atom at the other end, which has a varying side chain attached to it depending on the structure size. Spin density plots of selected radical product species have been shown in Fig. 7. For these structures, Table S10(a and b) (ESI†) include the molecular orbital plots, including the highest occupied molecular orbital (HOMO) and lowest occupied molecular orbital (LUMO) that correspond to these

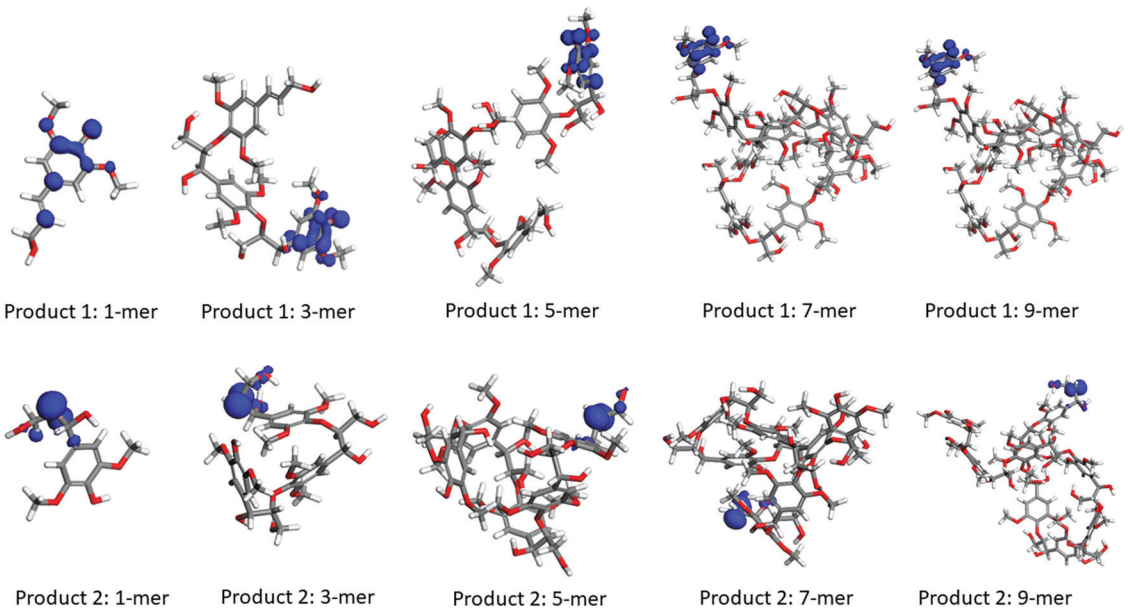

Fig. 7 Spin density plots with iso-value of 0.03 for selected free radical species studied in this work.

spin densities. The HOMO–LUMO energy gap was found to be related to the observed orbital plots for the radical species and the closed-shell molecule. In structures with a relatively large energy gap (1.2–1.58 eV), the HOMO was found at the opposite of the radical centers while the LUMO was found near the radical center. However, a smaller energy gap (0.5–0.6 eV) resulted in similar orbital plots in radical species. In product 1 structures, due to the presence of a strong electron-donating group, *i.e.*, an oxygen atom, the phenoxy radicals are well stabilized by the resonance throughout the conjugated system of π orbitals with delocalized electrons. Therefore, phenoxy radicals are more stabilized than the product 2 structures having secondary carbon-free radical centers. This trend can be seen in Fig. 7 of the spin density plots.

Since BDE values measure the stability of the radical products obtained from homolysis, our BDE calculations indicate the most stable radical products would form along pathways 3 and 4, which have the lowest BDE at a reference temperature of 298.15 K. The least stable radicals would be formed along pathway 1 and 7. The lowered BDE that has been found along pathways 3 and 4 are attributed to the increased bond length in β-O-4′ bonds, which decreased the bond strength. Subsequently, BDE decreased as well for these two pathways. On the other hand, pathways 1 and 7 have the highest two BDE values (72.14 kcal mol^{-1} and 76.41 kcal mol^{-1}, respectively), which correspond to the shorter bond length in β-O-4′ bonds for these two pathways. This finding aligns with our previous study, where we observed the different extent of radical stabilizations along the different reaction pathways.

Standard thermodynamic properties

In conventional thermodynamics, a physical property is any measurable property, the value of which describes a state of the system. Thermodynamic properties are the characteristic features that specify the system state. Hence, these properties are the pre-requisites for describing the behavior of any system. For the chemical industry, thermodynamic data at different process conditions are of key importance. Thermodynamic properties are obtained through experimental techniques, classical approaches, *i.e.*, equation of state and G^E model,[105] and computational approaches. Computational techniques derived from quantum chemistry and statistical mechanics predict molecular ensemble properties based on intra and inter-molecular interaction potentials. Estimating reaction kinetics involving radical species requires thermodynamic properties, which are not always available. Even though these transient species are present in trace quantity and disappear in a brief period of time, it is important to study their thermodynamic properties because the key intermediates for the majority of the reactions of organic molecules in the gas phase, such as the reaction being studied in the current work, are free radicals. Due to increased computational power at the present time, the range of molecules, both in terms of structure size and complexity, that can be studied computationally is growing rapidly. In this study, we have predicted standard thermodynamic properties including enthalpy of formation, heat capacity at constant pressure (C_p), entropy (S), and Gibbs free energy (G) for the closed-shell reactant molecule, which was a decamer, and all radical species, ranging from 1-mer to 9-mer.

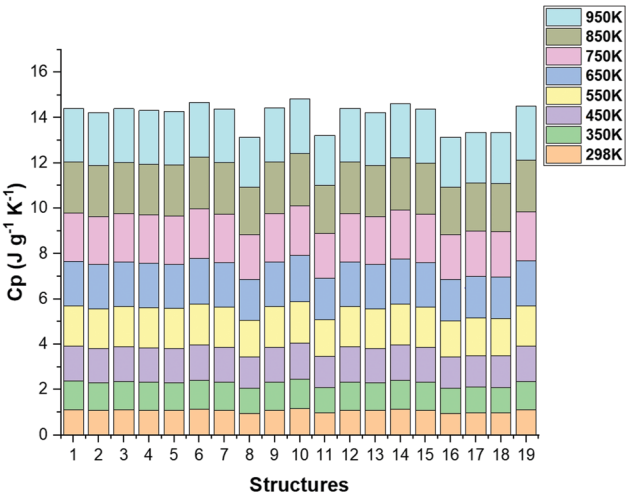

Fig. 8 Constant pressure heat capacity values for all structures in the current study at selected temperature. Structures 1–9 belong to product 1 starting from 1-mer to 9-mer with uniform increment in repeating unit. Similarly, structures 10–18 denote structures of varying sizes for product 2. Structure 19 denotes the reactant structure.

Constant pressure heat capacity

Fig. 8 shows the relationship with temperature for constant pressure heat capacity calculated for all the structures studied in this work. Over the range of temperature 25–1000 K, the monomer heat capacity values varied from 11.42–120.67 cal mol^{-1} K^{-1} for phenoxy radical species and 11.67–134.07 cal mol^{-1} K^{-1} for carbon-free radical species. For the 9-mers, the ranges obtained were 43.62–1172.79 and 41.50–1112.97 cal mol^{-1} K^{-1} for phenoxy and carbon-free radical structures, respectively. Our vibrational frequency calculations provided a range of 50.49–1311.76 cal mol^{-1} K^{-1} for the closed-shell reactant molecule (10-mer) over the same temperature range. While this range of Cp value was predicted for the hardwood model lignin in the current work, a range of 43.215–1115.082 cal mol^{-1} K^{-1} was predicted in our previous work for the softwood model lignin oligomer (10-mer). Heat capacity values have been obtained experimentally using an adiabatic calorimeter for softwood lignin using model compounds with molecular structure $C_{10}H_{11.9}O_{6.5}$ for cuproammonium lignin and $C_{10}H_{11.5}O_{3.9}$ for sulfuric lignin. Due to the proximity of the molecular formula for our softwood model lignin (*i.e.*, $C_{10}H_{12}O_{3.9}$) with these two model lignin compounds, we could validate our prediction for the heat capacity softwood model lignin with these experimentally obtained values. However, the repeating unit which has been used in this current study for hardwood lignin was $C_{11}H_{15}O_{4.9}$. Due to this dissimilarity in the repeating unit structure, we could not directly compare our predicted heat capacity values for hardwood model lignin. It is to be highlighted here that despite this dissimilarity in monomeric structures, predicted heat capacity

Table 4 Heat capacity for all species in this study for selected temperatures

(a)

Structure # (Reaction, Product Number: Name)	Molar mass (g mol^{-1})	C_p (J g^{-1} K^{-1}) Temperature (K) 298	350	450
1 (R1, P1: 1-mer)	209	1.11	1.26	1.54
2 (R2, P1: 2-mer)	435	1.07	1.23	1.52
3 (R3, P1: 3-mer)	661	1.09	1.25	1.54
4 (R4, P1: 4-mer)	887	1.08	1.24	1.53
5 (R5, P1: 5-mer)	1113	1.07	1.23	1.52
6 (R6, P1: 6-mer)	1339	1.12	1.28	1.57
7 (R7, P1: 7-mer)	1565	1.08	1.25	1.54
8 (R8, P1: 8-mer)	1791	0.95	1.10	1.38
9 (R9, P1: 9-mer)	2017	1.09	1.25	1.54
10 (R9, P2: 1-mer)	227	1.15	1.31	1.60
11 (R8, P2: 2-mer)	453	0.96	1.12	1.39
12 (R7, P2: 3-mer)	679	1.09	1.25	1.54
13 (R6, P2: 4-mer)	905	1.07	1.23	1.52
14 (R5, P2: 5-mer)	1131	1.12	1.28	1.57
15 (R4, P2: 6-mer)	1357	1.08	1.25	1.53
16 (R3, P2: 7-mer)	1583	0.95	1.10	1.38
17 (R2, P2: 8-mer)	1809	0.97	1.13	1.41
18 (R1, P2: 9-mer)	2035	0.97	1.13	1.41
19 (Reactant: 10-mer)	2244	1.10	1.26	1.55

(b)

Temperature (K)	C_p (J g^{-1} K^{-1}) 298	350	450
Cuproammonium lignin[106]	1.24	1.42	NA
Sulfuric lignin[106]	1.28	1.47	NA
Dioxane lignin[107]	NA	1.21	1.95
Softwood model lignin decamer[72] (previous study)	1.05	1.21	1.51
Hardwood model lignin decamer (current study)	1.10	1.26	1.55

values in this study are in closer proximity with these available reported experimental heat capacity values. These predictions would be more important at higher temperatures where experimental studies have more difficulty isolating reaction pathways due to complexity (Table 4).

Table 5 Calculated enthalpy of formation using atomization enthalpies for all species

Structure (reaction, product number: name)	Number of monomers	ΔH_f° (kJ mol^{-1})	Per monomer ΔH_f° (kJ mol^{-1})
R1, P1: 1-mer	1	−1299.67	−1299.67
R2, P1: 2-mer	2	−2992.02	−1499.51
R3, P1: 3-mer	3	−4722.93	−1574.31
R4, P1: 4-mer	4	−6471.07	−1617.77
R5, P1: 5-mer	5	−8193.54	−1638.71
R6, P1: 6-mer	6	−9904.83	−1650.81
R7, P1: 7-mer	7	−11528.28	−1646.90
R8, P1: 8-mer	8	−13370.86	−1671.36
R9, P1: 9-mer	9	−15094.65	−1677.18
R9, P2: 1-mer	1	−1535.18	−1535.18
R8, P2: 2-mer	2	−3049.34	−1524.67
R7, P2: 3-mer	3	−5067.09	−1689.03
R6, P2: 4-mer	4	−6730.05	−1682.51
R5, P2: 5-mer	5	−8437.56	−1687.51
R4, P2: 6-mer	6	−10237.88	−1706.31
R3, P2: 7-mer	7	−11985.94	−1712.27
R2, P2: 8-mer	8	−13660.23	−1707.53
R1, P2: 9-mer	9	−15313.97	−1701.56
Reactant: 10-mer	10	−16914.78	−1691.48

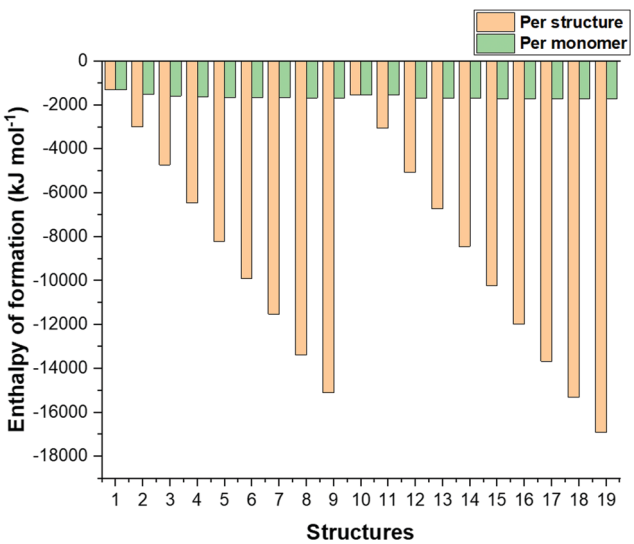

Fig. 9 Enthalpy of formation for all structures at reference temperature 298.15 K. Structures 1–9 belong to product 1 starting from 1-mer to 9-mer with uniform increment in repeating unit. Similarly, structures 10–18 denote structures of varying sizes for product 2. Structure 19 denotes the reactant structure.

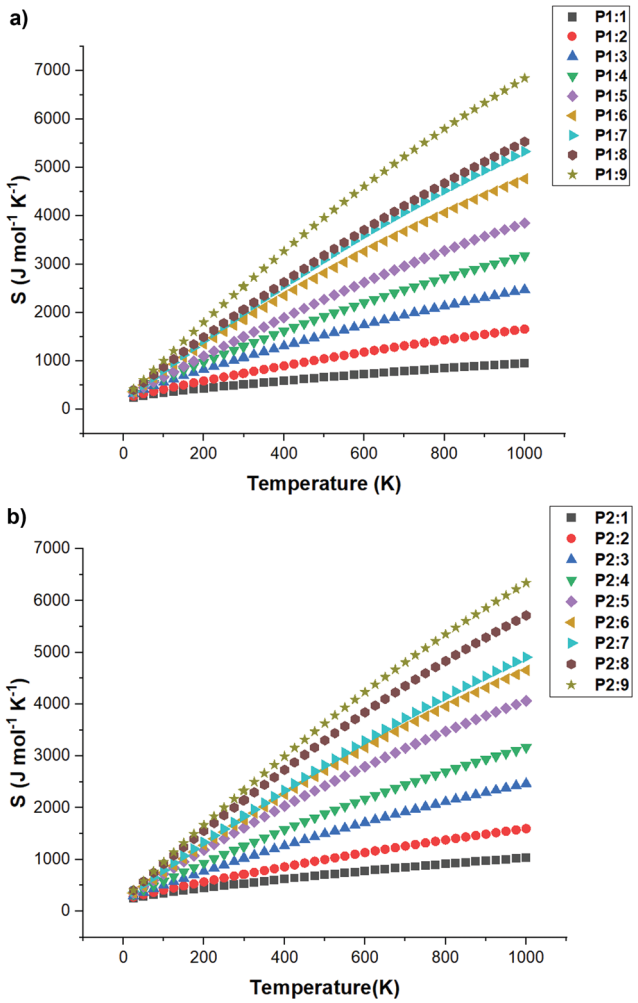

Fig. 10 (a) Entropy variation as a function of temperature for product 1 structures. Product 1 structures are phenoxy radicals and denoted as P1. The number after this notation indicates the number of monomers present in each of these structures. (b) Entropy variation as a function of temperature for product 2 structures. Product 2 structures are C free radicals and denoted as P2. The number after this notation indicates the number of monomers present in each of these structures.

Standard enthalpy of formation

From the context of pyrolysis, standard enthalpy of formation is one of the most important thermodynamic properties since it is closely related to the bond dissociation enthalpy. The atomization energy method for the calculation of enthalpy of formation requires the *ab initio* calculated enthalpy of atomization at 298 K and the experimental standard enthalpy of formation of atoms in the gas phase at the same temperature.[108] Following this approach, we calculated the enthalpy of formation values for the closed shell reactant decamer and the open shell product radicals, ranging from 1-mer to 9-mer (shown in Table 5). Our prediction for the enthalpy of formation for the hardwood model lignin decamer was −16914.7 kJ mol^{-1}. The range of enthalpy of formation values predicted for phenoxy radical products is (−1299.6 kJ mol^{-1})–(−1677.1 kJ mol^{-1}). A similar range of variation, *i.e.*, (−1535.1 kJ mol^{-1})–(−1701.5 kJ mol^{-1}), has been obtained for the carbon free radical species of varying sizes. Fig. 9 plots our prediction for enthalpies of formation including the corresponding values per monomer. The average heat of formation values per monomer was found to be −1626.87 kJ mol^{-1} with a standard deviation of 103.29. In our previous work with the softwood model lignin, the enthalpy of formation value per monomer was calculated as −762.1 kJ mol^{-1}, which we compared with the available experimental value, *i.e.*, −712.9 kJ mol^{-1}. In the absence of comparable experimental results for enthalpy of formation calculations, our predicted values would be very useful to be validated with the Benson's group additivity method for estimating heat of formation.[109]

Table 6 Calculated standard entropy values for all species

Structure (reaction, product number: name)	Number of monomers	S° (J mol^{-1} K^{-1})	Per monomer S° (J mol^{-1} K^{-1})
R1, P1: 1-mer	1	505.43	505.43
R2, P1: 2-mer	2	739.30	369.65
R3, P1: 3-mer	3	1065.04	355.02
R4, P1: 4-mer	4	1296.87	324.22
R5, P1: 5-mer	5	1495.29	299.06
R6, P1: 6-mer	6	1852.16	308.69
R7, P1: 7-mer	7	1997.16	285.31
R8, P1: 8-mer	8	2055.69	256.96
R9, P1: 9-mer	9	2531.87	281.32
R9, P2: 1-mer	1	532.23	532.23
R8, P2: 2-mer	2	711.95	355.98
R7, P2: 3-mer	3	1017.41	339.14
R6, P2: 4-mer	4	1254.84	313.71
R5, P2: 5-mer	5	1611.15	322.23
R4, P2: 6-mer	6	1767.77	294.63
R3, P2: 7-mer	7	1834.03	262.00
R2, P2: 8-mer	8	2141.72	267.71
R1, P2: 9-mer	9	2325.65	258.41
Reactant: 10-mer	10	2518.37	251.84
		Average	325.45

Entropy

The variation of standard entropy for all species of both radical types and the reactant molecule has been plotted as a function of temperature in Fig. 10(a and b). Table 6 reports the standard entropy values predicted for the reactant molecule and free radical species of the products in this study. Tables S4 and S5 (in ESI†) reports our prediction for entropy values for all species over the temperature range of 25–1000 K. The average value of standard entropy per monomer ($C_{11}H_{15}O_{4.9}$) in our calculation has been calculated as 325.43 J mol^{-1} K^{-1}. In our previous work with the softwood model lignin, the per monomer entropy value was found as 234.6 J mol^{-1} K^{-1} with a structural formula of $C_{10}H_{12}O_{3.9}$. This value was validated with the experimental work which reported 239.8 J mol^{-1} K^{-1} as the average entropy value per monomer for their model lignin compound.[106]

Conclusions

The presented work has used Density Functional Theory (DFT) electronic structure calculations at the BLYP/DNP level of theory to predict bond dissociation enthalpies (BDE) for the

homolytic cleavage of β-O-4′ linkage with a model lignin oligomer comprised of 10 Syringyl (S) units over a wide range of temperature from 25 K to 1000 K. As such, this work provides information on lignin pyrolysis chemistry with a model that is more representative of the hardwood lignin polymer than has been previously reported in the literature. Prior to DFT calculations, our work employed the conformational sampling method developed in our previous study to identify the lowest energy conformers for all free radical product species and the reactant molecule. Standard thermodynamic quantities, including enthalpy of formation, constant pressure heat capacity, entropy, and Gibbs free energy, have been predicted over the wide temperature range for all of the structures.

• Marked position dependence was found in the computed BDEs, which provides insight for the overall understanding of the homolytic cleavage of β-O-4′ reaction, a barrierless reaction during lignin pyrolysis. Due to the exponential dependence of the reaction rate coefficients on the activation energy, which is the reaction enthalpy for this barrierless reaction, reporting of this position dependence of BDEs provides meaningful insights to communities seeking reaction energetics for lignin-related species. The range of the BDEs predicted in this study using quantum mechanical calculations would be very useful to design reactors for biomass pyrolysis with a higher hardwood lignin content.

• The present study indicates that the BDEs are higher in hardwood lignin than softwood lignin. For all the reaction pathways, the mean BDEs have been slightly higher in this study with the hardwood lignin model than that of the softwood model lignin in our previous study. Since the model has not included other linkages or monolignols, this study has isolated the methoxy group role in the reaction energetics of lignin pyrolysis.

• Our calculated values for standard thermodynamic properties would be beneficial for cross-validation with experimental studies. Similar to the reaction energetics calculations, this study isolates the effect of syringyl monolignol in thermodynamic properties during biomass pyrolysis. Because two different model structures have been used in this study for hardwood lignin and our previous study for softwood lignin, the predicted thermodynamic properties provide a systematic comparison of structural effects on thermochemistry for lignin-related species.

Overall, these insights and predictions provide new information to be used for reactor design, kinetic modeling, and process optimization efforts to increase product selectivity and yield for a biomass feedstock with higher hardwood lignin content.

Conflicts of interest

There are no conflicts to declare.

Acknowledgements

We are grateful for the support of this work by the Alabama Supercomputing Center, Auburn University Hopper high-performance compute cluster resources, USDA grant 18-JV-11330131-073 and Auburn University new faculty start-up funding.

References

1 M. Y. Balakshin, E. A. Capanema, I. Sulaeva, P. Schlee, Z. E. Huang, M. Feng, M. Borghei, O. J. Rojas, A. Potthast and T. Rosenau, New opportunities in the valorization of technical lignins, *ChemSusChem*, 2020, **22**, DOI: 10.1002/cssc.202002553.

2 O. Y. Abdelaziz and C. P. Hulteberg, Lignin depolymerization under continuous-flow conditions: Highlights of recent developments, *ChemSusChem*, 2020, **13**(17), 4382–4384.

3 X. Du, H. C. Zhang, K. P. Sullivan, P. Gogoi and Y. L. Deng, Electrochemical lignin conversion, *ChemSusChem*, 2020, **13**(17), 4318–4343.

4 Y. X. Jing, L. Dong, Y. Guo, X. H. Liu and Y. Q. Wang, Chemicals from lignin: A review of catalytic conversion involving hydrogen, *ChemSusChem*, 2020, **13**(17), 4181–4198.

5 Z. H. Sun, B. Fridrich, A. de Santi, S. Elangovan and K. Barta, Bright side of lignin depolymerization: Toward new platform chemicals, *Chem. Rev.*, 2018, **118**(2), 614–678.

6 P. Alvira, E. Tomas-Pejo, M. Ballesteros and M. J. Negro, Pretreatment technologies for an efficient bioethanol production process based on enzymatic hydrolysis: A review, *Bioresour. Technol.*, 2010, **101**(13), 4851–4861.

7 Y. H. P. Zhang and L. R. Lynd, Toward an aggregated understanding of enzymatic hydrolysis of cellulose: Noncomplexed cellulase systems, *Biotechnol. Bioeng.*, 2004, **88**(7), 797–824.

8 J. A. Langston, T. Shaghasi, E. Abbate, F. Xu, E. Vlasenko and M. D. Sweeney, Oxidoreductive cellulose depolymerization by the enzymes cellobiose dehydrogenase and glycoside hydrolase 61, *Appl. Environ. Microbiol.*, 2011, **77**(19), 7007–7015.

9 Z. M. Zhao, Z. H. Liu, Y. Q. Pu, X. Z. Meng, J. F. Xu, J. S. Yuan and A. J. Ragauskas, Emerging strategies for modifying lignin chemistry to enhance biological lignin valorization, *ChemSusChem*, 2020, **13**(20), 5423–5432.

10 S. Yu, H. M. Brown, X. W. Huang, X. D. Zhou, J. E. Amonette and Z. C. Zhang, Single-step conversion of cellulose to 5-hydroxymethylfurfural (HMF), a versatile platform chemical, *Appl. Catal., A*, 2009, **361**(1–2), 117–122.

11 J. S. Luterbacher, D. M. Alonso, J. M. Rand, Y. M. Questell-Santiago, J. H. Yeap, B. F. Pfleger and J. A. Dumesic, Solvent-enabled nonenyzmatic sugar production from biomass for chemical and biological upgrading, *ChemSusChem*, 2015, **8**(8), 1317–1322.

12 D. M. Alonso, S. G. Wettstein and J. A. Dumesic, Bimetallic catalysts for upgrading of biomass to fuels and chemicals, *Chem. Soc. Rev.*, 2012, **41**(24), 8075–8098.

13 S. Van De Vyver, J. Geboers, P. A. Jacobs and B. F. Sels, Recent advances in the catalytic conversion of cellulose, *ChemCatChem*, 2011, **3**(1), 82–94.

14 X. D. Liu, F. P. Bouxin, J. J. Fan, V. L. Budarin, C. W. Hu and J. H. Clark, Recent advances in the catalytic depolymerization of lignin towards phenolic chemicals: A review, *ChemSusChem*, 2020, **13**(17), 4296–4317.
15 H. L. Zhu, W. Luo, P. N. Ciesielski, Z. Q. Fang, J. Y. Zhu, G. Henriksson, M. E. Himmel and L. B. Hu, Wood-derived materials for green electronics, biological devices, and energy applications, *Chem. Rev.*, 2016, **116**(19), 12650.
16 A. Gonzalez-Quiroga, M. R. Djokic, K. M. Van Geem and G. B. Marin, Conversion of solid waste to diesel via catalytic pressureless depolymerization: Pilot scale production and detailed compositional characterization, *Energy Fuels*, 2016, **30**(10), 8292–8303.
17 M. Barde, C. W. Edmunds, N. Labbe and M. L. Auad, Fast pyrolysis bio-oil from lignocellulosic biomass for the development of bio-based cyanate esters and cross-linked networks, *High Perform. Polym.*, 2019, **31**(9–10), 1140–1152.
18 M. Barde, K. Avery, C. W. Edrnunds, N. Labbe and M. L. Auad, Cross-linked acrylic polymers from the aqueous phase of biomass pyrolysis oil and acrylated epoxidized soybean oil, *ACS Sustainable Chem. Eng.*, 2019, **7**(2), 2216–2224.
19 B. S. Hernandez, M. Barde, B. Via and M. L. Auad, Sustainable products from bio-oils., *MRS Bull.*, 2017, **42**(5), 365–370.
20 S. Al Arni, B. Bosio and E. Arato, Syngas from sugarcane pyrolysis: An experimental study for fuel cell applications, *Renewable Energy*, 2010, **35**(1), 29–35.
21 A. J. A. van Maris, D. A. Abbott, E. Bellissimi, J. van den Brink, M. Kuyper, M. A. H. Luttik, H. W. Wisselink, W. A. Scheffers, J. P. van Dijken and J. T. Pronk, Alcoholic fermentation of carbon sources in biomass hydrolysates by Saccharomyces cerevisiae: Current status, *Antonie van Leeuwenhoek*, 2006, **90**(4), 391–418.
22 D. Tarasov, M. Leitch and P. Fatehi, Lignin-carbohydrate complexes: Properties, applications, analyses, and methods of extraction: A review, *Biotechnol. Biofuels*, 2018, **11**, 28.
23 T. Higuchi, *Biosynthesis of lignin*, 1985, 141–160.
24 J. J. Stewart, T. Akiyama, C. Chapple, J. Ralph and S. D. Mansfield, The effects on lignin structure of overexpression of ferulate 5-hydroxylase in hybrid poplar, *Plant Physiol.*, 2009, **150**(2), 621–635.
25 J. M. Humphreys and C. Chapple, Rewriting the lignin roadmap, *Curr. Opin. Plant Biol.*, 2002, **5**(3), 224–229.
26 T. Elder, J. C. del Rio, J. Ralph, J. Rencoret, H. Kim and G. T. Beckham, Radical coupling reactions of piceatannol and monolignols: A density functional theory study, *Phytochemistry*, 2019, **164**, 12–23.
27 R. R. Sederoff, J. J. MacKay, J. Ralph and R. D. Hatfield, Unexpected variation in lignin, *Curr. Opin. Plant Biol.*, 1999, **2**(2), 145–152.
28 R. Vanholme, K. Morreel, J. Ralph and W. Boerjan, Lignin engineering, *Curr. Opin. Plant Biol.*, 2008, **11**(3), 278–285.
29 R. Vanholme, K. Morreel, C. Darrah, P. Oyarce, J. H. Grabber, J. Ralph and W. Boerjan, Metabolic engineering of novel lignin in biomass crops, *New Phytol.*, 2012, **196**(4), 978–1000.
30 R. Vanholme, B. De Meester, J. Ralph and W. Boerjan, Lignin biosynthesis and its integration into metabolism, *Curr. Opin. Biotechnol.*, 2019, **56**, 230–239.
31 E. Adler, Lignin chemistry – past, present and future, *Wood Sci. Technol.*, 1977, **11**(3), 169–218.
32 Y. Kojima, S. Isaji, S. L. Yoon and T. Ona, Selection criteria of *Eucalyptus globulus* Labill for production of chemithermomechanical pulps (CTMP), *Holzforschung*, 2008, **62**(1), 71–76.
33 I. Miranda and H. Pereira, The variation of chemical composition and pulping yield with age and growth factors in young *Eucalyptus globulus*, *Wood Fiber Sci.*, 2002, **34**(1), 140–145.
34 J. Rencoret, A. Gutierrez, L. Nieto, J. Jimenez-Barbero, C. B. Faulds, H. Kim, J. Ralph, A. T. Martinez and J. C. del Rio, Lignin composition and structure in young *versus* adult eucalyptus globulus plants, *Plant Physiol.*, 2011, **155**(2), 667–682.
35 S. Van den Bosch, W. Schutyser, R. Vanholme, T. Driessen, S. F. Koelewijn, T. Renders, B. De Meester, W. J. J. Huijgen, W. Dehaen, C. M. Courtin, B. Lagrain, W. Boerjan and B. F. Sels, Reductive lignocellulose fractionation into soluble lignin-derived phenolic monomers and dimers and processable carbohydrate pulps, *Energy Environ. Sci.*, 2015, **8**(6), 1748–1763.
36 T. Renders, G. Van den Bossche, T. Vangeel, K. Van Aelst and B. Sels, Reductive catalytic fractionation: State of the art of the lignin-first biorefinery, *Curr. Opin. Biotechnol.*, 2019, **56**, 193–201.
37 R. T. Davis, L. Tan, E. C. D. Biddy, M. J. Beckham, G. T. Scarlata, C. Jacobson, J. Cafferty, K. Ross, J. Lukas, J. Knorr and D. Schoen, *Process design and economics for the conversion of lignocellulosic biomass to hydrocarbons:Dilute-acid and enzymatic deconstruction of biomass to sugars and biological conversion of sugars to hydrocarbons*, NREL, 2013.
38 S. R. Wang, G. X. Dai, H. P. Yang and Z. Y. Luo, Lignocellulosic biomass pyrolysis mechanism: A state-of-the-art review, *Prog. Energy Combust. Sci.*, 2017, **62**, 33–86.
39 P. R. Patwardhan, R. C. Brown and B. H. Shanks, Understanding the fast pyrolysis of lignin, *ChemSusChem*, 2011, **4**(11), 1629–1636.
40 Q. Liu, S. R. Wang, Y. Zheng, Z. Y. Luo and K. F. Cen, Mechanism study of wood lignin pyrolysis by using TG-FTIR analysis, *J. Anal. Appl. Pyrol.*, 2008, **82**(1), 170–177.
41 H. Cheng, S. B. Wu and C. Liu, Study on the mechanism of the pyrolysis of a lignin monomeric model compound by *in situ* FTIR, *BioResources*, 2014, **9**(3), 4441–4448.
42 M. W. J. Tian, D. MacDonald, M. R. Asmussen and A. Chen, A novel approach for lignin modification and degradation, *Electrochem. Commun.*, 2010, **12**(4), 527–530.
43 A. D. Paulsen, B. R. Hough, C. L. Williams, A. R. Teixeira, D. T. Schwartz, J. Pfaendtner and P. J. Dauenhauer, Fast pyrolysis of wood for biofuels: Spatiotemporally resolved diffuse reflectance in situ spectroscopy of particles, *ChemSusChem*, 2014, **7**(3), 765–776.
44 A. Dufour, M. Castro-Diaz, P. Marchal, N. Brosse, R. Olcese, M. Bouroukba and C. Snape, *In situ* analysis of biomass

pyrolysis by high temperature rheology in relations with H-1 NMR, *Energy Fuels*, 2012, **26**(10), 6432–6441.

45 H. Kawamoto, M. Ryoritani and S. Saka, Different pyrolytic cleavage mechanisms of beta-ether bond depending on the side-chain structure of lignin dimers, *J. Anal. Appl. Pyrol.*, 2008, **81**(1), 88–94.

46 H. Kawamoto, S. Horigoshi and S. Saka, Pyrolysis reactions of various lignin model dimers, *J. Wood Sci.*, 2007, **53**(2), 168–174.

47 H. Kawamoto, S. Horigoshi and S. Saka, Effects of side-chain hydroxyl groups on pyrolytic beta-ether cleavage of phenolic lignin model dimer, *J. Wood Sci.*, 2007, **53**(3), 268–271.

48 H. Kawamoto, T. Nakamura and S. Saka, Pyrolytic cleavage mechanisms of lignin-ether linkages: A study on p-substituted dimers and trimers, *Holzforschung*, 2008, **62**(1), 50–56.

49 Y. Uraki, Y. Sugiyama, K. Koda, S. Kubo, T. Kishimoto and J. F. Kadla, Thermal mobility of beta-*o*-4-type artificial lignin., *Biomacromolecules*, 2012, **13**(3), 867–872.

50 T. Kishimoto, Y. Uraki and M. Ubukata, Easy synthesis of beta-O-4 type lignin related polymers, *Org. Biomol. Chem.*, 2005, **3**(6), 1067–1073.

51 T. Kishimoto, Y. Uraki and M. Ubukata, Chemical synthesis of beta-O-4 type artificial lignin, *Org. Biomol. Chem.*, 2006, **4**(7), 1343–1347.

52 T. Kishimoto, Y. Uraki and M. Ubukata, Synthesis of beta-*O*-4-type artificial lignin polymers and their analysis by NMR spectroscopy, *Org. Biomol. Chem.*, 2008, **6**(16), 2982–2987.

53 B. Hu, B. Zhang, W. L. Xie, X. Y. Jiang, J. Liu and Q. Lu, Recent progress in quantum chemistry modeling on the pyrolysis mechanisms of lignocellulosic biomass, *Energy Fuels*, 2020, **34**(9), 10384–10440.

54 C. Chen, L. L. Zhao, J. F. Wang and S. C. Lin, Reactive molecular dynamics simulations of biomass pyrolysis and combustion under various oxidative and humidity environments, *Ind. Eng. Chem. Res.*, 2017, **56**(43), 12276–12288.

55 T. T. Zhang, X. X. Li and L. Guo, Initial reactivity of linkages and monomer rings in lignin pyrolysis revealed by ReaxFF molecular dynamics, *Langmuir*, 2017, **33**(42), 11646–11657.

56 T. T. Zhang, X. X. Li, L. Gao and X. Guo, Reaction mechanisms in pyrolysis of hardwood, softwood, and kraft lignin revealed by ReaxFF MD simulations, *Energy Fuels*, 2019, **33**(11), 11210–11225.

57 R. Parthasarathi, R. A. Romero, A. Redondo and S. Gnanakaran, Theoretical study of the remarkably diverse linkages in lignin, *J. Phys. Chem. Lett.*, 2011, **2**(20), 2660–2666.

58 S. Kim, S. C. Chmely, M. R. Nimos, Y. J. Bomble, T. D. Foust, R. S. Paton and G. T. Beckham, Computational study of bond dissociation enthalpies for a large range of native and modified lignins, *J. Phys. Chem. Lett.*, 2011, **2**(22), 2846–2852.

59 T. Elder, Bond dissociation enthalpies of a dibenzodioxocin lignin model compound, *Energy Fuels*, 2013, **27**(8), 4785–4790.

60 T. Elder, Bond dissociation enthalpies of a pinoresinol lignin model compound, *Energy Fuels*, 2014, **28**(2), 1175–1182.

61 T. Elder and A. Beste, Density functional theory study of the concerted pyrolysis mechanism for lignin models, *Energy Fuels*, 2014, **28**(8), 5229–5235.

62 M. T. Klein and P. S. Virk, Model pathways in lignin thermolysis. 1. Phenethyl phenyl ether, *Ind. Eng. Chem. Fundam.*, 1983, **22**(1), 35–45.

63 M. W. Jarvis, J. W. Daily, H. H. Carstensen, A. M. Dean, S. Sharma, D. C. Dayton, D. J. Robichaud and M. R. Nimlos, Direct detection of products from the pyrolysis of 2-phenethyl phenyl ether, *J. Phys. Chem. A*, 2011, **115**(4), 428–438.

64 T. Kishimoto and Y. Sano, Delignification mechanism during high-boiling solvent pulping – Part 2. Homolysis of guaiacylglycerol-beta-guaiacyl ether, *Holzforschung*, 2002, **56**(6), 623–631.

65 S. Li and K. Lundquist, Reactions of the beta-aryl ether lignin model 1-(4-hydroxy-3-methoxyphenyl)-2-(2-methoxyphenoxy)-1-propanol on heating in aqueous solution, *Holzforschung*, 2001, **55**(3), 296–301.

66 M. Tanahashi, M. Karina, K. Tamabuchi and T. Higuchi, Degradation mechanism of lignin accompanying steam explosions. 1. degradation products of lignin and beta-o-4 lignin substructure model dimers, *Mokuzai Gakkaishi*, 1989, **35**(2), 135–143.

67 Q. R. Shen, Z. W. Fu, R. Li and Y. L. Wu, A study on the pyrolysis mechanism of a beta-O-4 lignin dimer model compound using DFT combined with Py-GC/MS, *J. Therm. Anal. Calorim.*, 2020, **11**, DOI: 10.1007/s10973-020-10130-1.

68 S. M. Li, Z. Y. Luo, W. B. Wang, K. Y. Lu, Y. Yang and X. R. Liang, Characterization of pyrolytic lignin and insight into its formation mechanisms using novel techniques and DFT method, *Fuel*, 2020, **262**, 11.

69 M. Rashidi, J. N. Beltramini and D. Martin, The selective cleavage of lignin aliphatic C–O linkages by solvent-assisted fast pyrolysis (SAFP), *J. Incl. Phenom. Macrocycl. Chem.*, 2019, **94**(3-4), 297–307.

70 L. Shuai, J. Sitison, S. Sadula, J. H. Ding, M. C. Thies and B. Saha, Selective C-C bond cleavage of methylene-linked lignin models and kraft lignin., *ACS Catal.*, 2018, **8**(7), 6507–6512.

71 W. K. Jiang and S. B. Wu, Mechanism study on depolymerization of the alpha-o-4 linkage lignin model compound in supercritical ethanol system, *Waste Biomass Valorization*, 2019, **10**(1), 197–204.

72 T. Azad, J. D. Schuler, M. L. Auad, T. Elder and A. J. Adamczyk, Model lignin oligomer pyrolysis: Coupled conformational andthermodynamic analysis of β-O-4′ bond cleavage, *Energy Fuels*, 2020, 9709–9724.

73 M. J. Orella, T. Z. H. Gani, J. V. Vermaas, M. L. Stone, E. M. Anderson, G. T. Beckham, F. R. Brushett and Y. Roman-Leshkov, Lignin-KMC: A toolkit for simulating lignin biosynthesis, *ACS Sustainable Chem. Eng.*, 2019, **7**(22), 18313–18322.

74 V. B. F. Custodis, P. Hemberger, Z. Q. Ma and J. A. van Bokhoven, Mechanism of fast pyrolysis of lignin: Studying model compounds, *J. Phys. Chem. B*, 2014, **118**(29), 8524–8531.
75 V. B. F. Custodis, P. Hemberger and J. A. van Bokhoven, How inter- and intramolecular reactions dominate the formation of products in lignin pyrolysis, *Chem. – Eur. J.*, 2017, **23**(36), 8658–8668.
76 N. Metropolis, A. W. Rosenbluth, M. N. Rosenbluth, A. H. Teller and E. Teller, Equation of state calculations by fast computing machines, *J. Chem. Phys.*, 1953, **21**(6), 1087–1092.
77 J. P. Perdew, K. Burke and M. Ernzerhof, Generalized gradient approximation made simple (vol. 77, p. 3865, 1996), *Phys. Rev. Lett.*, 1997, **78**(7), 1396.
78 Y. Inada and H. Orita, Efficiency of numerical basis sets for predicting the binding energies of hydrogen bonded complexes: Evidence of small basis set superposition error compared to Gaussian basis sets, *J. Comput. Chem.*, 2008, **29**(2), 225–232.
79 A. J. Adamczyk, M. F. Reyniers, G. B. Marin and L. J. Broadbelt, Hydrogenated amorphous silicon nanostructures: novel structure-reactivity relationships for cyclization and ring opening in the gas phase, *Theor. Chem. Acc.*, 2011, **128**(1), 91–113.
80 S. D. Deng, G. B. Du, X. H. Li and X. G. Xie, Performance, reaction mechanism, and characterization of glyoxal-monomethylol urea (G-MMU) resin, *Ind. Eng. Chem. Res.*, 2014, **53**(13), 5421–5431.
81 B. S. Tan, R. F. Peng, H. B. Li, B. Jin, S. J. Chu and X. P. Long, Theoretical investigation of an energetic fullerene derivative, *J. Comput. Chem.*, 2010, **31**(12), 2233–2237.
82 J. Q. Wang, L. L. Liu and A. K. Wilson, Oxidative cleavage of the beta-O-4 linkage of lignin by transition metals: Catalytic properties and the performance of density functionals, *J. Phys. Chem. A*, 2016, **120**(5), 737–746.
83 T. van Mourik, V. I. Danilov, V. V. Dailidonis, N. Kurita, H. Wakabayashi and T. Tsukamoto, A DFT study of uracil and 5-bromouracil in nanodroplets, *Theor. Chem. Acc.*, 2010, **125**(3–6), 233–244.
84 A. Tkatchenko and M. Scheffler, Accurate molecular van der Waals interactions from ground-state electron density and free-atom reference data, *Phys. Rev. Lett.*, 2009, **102**(7), 4.
85 A. J. Adamczyk and L. J. Broadbelt, Thermochemical property estimation of hydrogenated silicon clusters, *J. Phys. Chem. A*, 2011, **115**(32), 8969–8982.
86 A. J. Adamczyk, M. F. Reyniers, G. B. Marin and L. J. Broadbelt, Exploring 1,2-hydrogen shift in silicon nanoparticles: Reaction kinetics from quantum chemical calculations and derivation of transition state group additivity database, *J. Phys. Chem. A*, 2009, **113**(41), 10933–10946.
87 A. J. Adamczyk, M. F. Reyniers, G. B. Marin and L. J. Broadbelt, Kinetics of substituted silylene addition and elimination in silicon nanocluster growth captured by group additivity, *ChemPhysChem.*, 2010, **11**(9), 1978–1994.
88 A. J. Adamczyk, M. F. Reyniers, G. B. Marin and L. J. Broadbelt, Kinetic correlations for H-2 addition and elimination reaction mechanisms during silicon hydride pyrolysis, *Phys. Chem. Chem. Phys.*, 2010, **12**(39), 12676–12696.
89 A. J. Adamczyk and L. J. Broadbelt, The role of multifunctional kinetics during early-stage silicon hydride pyrolysis: Reactivity of Si2H2 isomers with SiH4 and Si2H6, *J. Phys. Chem. A*, 2011, **115**(11), 2409–2422.
90 D. A. McQuarrie, *Statistical Mechanics.*, Harper & Row:, 1973.
91 J. A. Pople, M. Headgordon and K. Raghavachari, Quadratic configuration-interaction – a general technique for determining electron correlation energies, *J. Chem. Phys.*, 1987, **87**(10), 5968–5975.
92 G. D. Purvis and R. J. Bartlett, A full coupled-cluster singles and doubles model – the inclusion of disconnected triples, *J. Chem. Phys.*, 1982, **76**(4), 1910–1918.
93 G. E. Scuseria, C. L. Janssen and H. F. Schaefer, An efficient reformulation of the closed-shell coupled cluster single and double excitation (CCSD) equations, *J. Chem. Phys.*, 1988, **89**(12), 7382–7387.
94 G. E. Scuseria and H. F. Schaefer, Is coupled cluster singles and doubles (CCSD) more computationally intensive than quadratic configuration-interaction (QCISD), *J. Chem. Phys.*, 1989, **90**(7), 3700–3703.
95 L. A. Curtiss, K. Raghavachari, G. W. Trucks and J. A. Pople, Gaussian-2 theory for molecular-energies of 1st-row and 2nd-row compounds, *J. Chem. Phys.*, 1991, **94**(11), 7221–7230.
96 L. A. Curtiss, K. Raghavachari, P. C. Redfern, V. Rassolov and J. A. Pople, Gaussian-3 (G3) theory for molecules containing first and second-row atoms, *J. Chem. Phys.*, 1998, **109**(18), 7764–7776.
97 G. A. DiLabio, D. A. Pratt, A. D. LoFaro and J. S. Wright, Theoretical study of X–H bond energetics (X = C, N, O, S): Application to substituent effects, gas phase acidities, and redox potentials, *J. Phys. Chem. A*, 1999, **103**(11), 1653–1661.
98 E. R. Johnson and A. D. Becke, A unified density-functional treatment of dynamical, nondynamical, and dispersion correlations. II. Thermochemical and kinetic benchmarks, *J. Chem. Phys.*, 2008, **128**(12), 3.
99 G. A. DiLabio, Using locally dense basis sets for the determination of molecular properties, *J. Phys. Chem. A*, 1999, **103**(51), 11414–11424.
100 J. P. Senosiain, J. H. Han, C. B. Musgrave and D. M. Golden, Use of quantum methods for a consistent approach to combustion modelling: Hydrocarbon bond dissociation energies, *Faraday Discss.*, 2002, **119**, 173–189.
101 Y. Feng, L. Liu, J. T. Wang, H. Huang and Q. X. Guo, Assessment of experimental bond dissociation energies using composite ab initio methods and evaluation of the performances of density functional methods in the

calculation of bond dissociation energies, *J. Chem. Inf. Comput. Sci.*, 2003, **43**(6), 2005–2013.

102 J. B. Huang, C. Liu, Q. J. Jin, H. Tong, W. M. Li and D. Wu, Density functional theory study on bond dissociation enthalpies for lignin dimer model compounds, *J. Renewable Sustainable Energy*, 2014, **6**(3), 8.

103 H. J. Z. Y. Wang, C. Wang, Y. Fu and Q. X. Guo, Theoretical study on the pyrolysis process of lignin dimer model compounds, *Acta Chim. Sin.*, 2009, **67**(9), 893–900.

104 J. J. Zhang, X. Y. Jiang, X. N. Ye, L. Chen, Q. Lu, X. H. Wang and C. Q. Dong, Pyrolysis mechanism of a beta-O-4 type lignin dimer model compound, *J. Therm. Anal. Calorim.*, 2016, **123**(1), 501–510.

105 B. E. P. Poling, J. M. Prausnitz and J. P. O'Connell, *The properties of gases and liquids*, McGraw-Hill Education, 2000, p. 768.

106 O. V. Voitkevich, G. J. Kabo, A. V. Blokhin, Y. U. Paulechka and M. V. Shishonok, Thermodynamic properties of plant biomass components. Heat capacity, combustion energy, and gasification equilibria of lignin, *J. Chem. Eng. Data*, 2012, **57**(7), 1903–1909.

107 T. Hatakeyama, K. Nakamura and H. Hatakeyama, Studies on heat-capacity of cellulose and lignin by differential scanning calorimetry, *Polymer*, 1982, **23**(12), 1801–1804.

108 A. Ince, H. H. Carstensen, M. F. Reyniers and G. B. Marin, First-principles based group additivity values for thermochemical properties of substituted aromatic compounds, *AIChE J.*, 2015, **61**(11), 3858–3870.

109 S. W. C. Benson, F. R. Cruickshank, D. M. Golden, G. R. Haugen, E. O'neal, A. S. Rodgers, R. Shaw and R. Walsh, Additivity rules for estimation of thermochemical properties, *J. Chem. Phys.*, 1958, 29.